Preventing Interfacial Recombination in Colloidal Quantum Dot Solar Cells by Doping the Metal Oxide

Bruno Ehrler,[†,§] Kevin P. Musselman,[†,§] Marcus L. Böhm,[†] Frederik S. F. Morgenstern,[†] Yana Vaynzof,[†] Brian J. Walker,[†] Judith L. MacManus-Driscoll,[‡] and Neil C. Greenham[†,*]

[†]Cavendish Laboratory, University of Cambridge, J.J. Thomson Avenue, Cambridge CB3 0HE, U.K., and [‡]Department of Materials Science, University of Cambridge, Pemroke Street, Cambridge, CB2 3QZ, U.K. [§]B. Ehrler and K. P. Musselman contributed equally.

ABSTRACT Recent research has pushed the efficiency of colloidal quantum dot solar cells toward a level that spurs commercial interest. Quantum dot/metal oxide bilayers form the most efficient colloidal quantum dot solar cells, and most studies have advanced the understanding of the quantum dot component. We study the interfacial recombination process in depleted heterojunction colloidal quantum dot (QD) solar cells formed with ZnO as the oxide by varying (i) the carrier concentration of the ZnO layer and (ii) the density of intragap recombination sites in the QD layer. We find that the open-circuit voltage and efficiency of PbS QD/ZnO devices can be improved by 50% upon doping of the ZnO with nitrogen to reduce its carrier concentration. In contrast, doping the ZnO did not change the performance of PbSe QD/ZnO solar cells. We use X-ray photoemission spectroscopy, ultraviolet photoemission spectroscopy, transient photovoltage decay measurements, transient absorption spectroscopy, and intensity-dependent photocurrent measurements to investigate the origin of this effect. We find a significant density of intragap states within the band gap of the PbS quantum dots. These states facilitate recombination at the PbS/ZnO interface, which can be suppressed by reducing the density of occupied states in the ZnO. For the PbSe QD/ZnO solar cells, where fewer intragap states are observed in the quantum dots, the interfacial recombination channel does not limit device performance. Our study sheds light on the mechanisms of interfacial recombination in colloidal quantum dot solar cells and emphasizes the influence of quantum dot intragap states and metal oxide properties on this loss pathway.

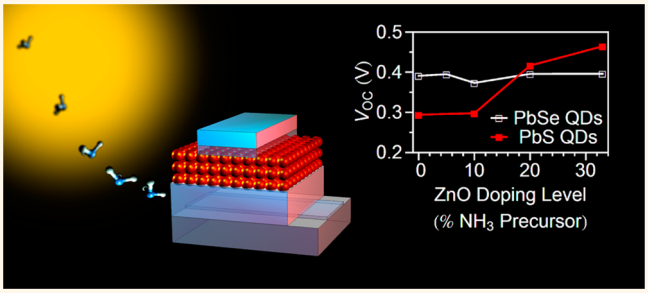

KEYWORDS: metal oxide · colloidal quantum dot solar cells · intragap states · solar cell · recombination

Semiconducting quantum dots (QDs) have attracted considerable attention as key materials in optoelectronic devices including light-emitting diodes,[1] field-effect transistors,[2] photodetectors,[3,4] and photovoltaics.[5,6] They offer important advantages over conventional bulk materials such as solution-processability, low-temperature fabrication, and quantum size-effect tunability of their band gap, which allows their absorption properties to be optimized for photovoltaic applications. Quantum dot/metal oxide heterojunctions have been introduced recently and offer several advantages over previous photovoltaic architectures. Their inverted structure enables the use of a stable, high-workfunction electrode and positions the charge-separating quantum dot/metal oxide interface at the front of the cell.[7,8] In addition, the valence band offset provides a barrier for hole injection into the acceptor. This has been demonstrated in systems consisting of n-type zinc oxide (ZnO) and p-type lead chalcogenide quantum dots,[9−11] resulting in peak efficiencies of 4.7% for devices displaying carrier multiplication effects.[12] Research in these quantum dot/metal oxide based solar cells has focused mainly on the properties of the quantum dot component.[9,13−15] Of the studies that focus on the metal oxide properties, most deal with morphological optimization of the interface.[16,17] Tuning of the electrical properties of the metal oxide has received considerably less attention, but may be similarly important. For instance, Liu *et al.* doped TiO_2 films to optimize energy alignment at the quantum dot/metal

* Address correspondence to ncg11@cam.ac.uk.

Received for review February 6, 2013 and accepted March 26, 2013.

Published online March 26, 2013
10.1021/nn400656n

oxide interface and improve minority carrier injection from the quantum dot film.[18] Here we study the influence of ZnO carrier concentration on the performance of PbX (X = S, Se) QD/ZnO solar cells (architecture shown in Figure 1a) by doping the ZnO with nitrogen (N:ZnO). We identify trap-assisted interfacial recombination as a major loss channel in the PbS/ZnO system and demonstrate a 50% improvement in open-circuit voltage when charge carrier densities in the ZnO are adjusted to limit this recombination.

Quantum dot/metal oxide bilayer devices are expected to result in a depleted-heterojunction structure.[7] To estimate the band structure, an effective medium picture is assumed, whereby representative bulk properties are used to describe the quantum dot layer. Carrier concentrations around 10^{16} to 10^{17} cm^{-3} are typically reported for PbS and PbSe quantum dots.[5,19−21] Commonly used oxides, on the other hand, are characterized by higher carrier concentrations, *e.g.*, 10^{17} to 10^{20} cm^{-3},[22−25] due to shallow intrinsic donors such as zinc interstitials and oxygen vacancies in ZnO.[26] It follows that the built-in potential is accommodated almost entirely in the quantum dot layers, as shown in Figure 1b. It is believed that photogenerated excitons are dissociated by the built-in field in the quantum dot layer, and electrons and holes are transported by drift and diffusion to the collection electrodes.[7] Recombination is known to occur in the quantum dot layer *via* trap-assisted recombination, Auger processes, and radiative decay, as shown in Figure 1c (ii)−(iv).[27−29] Due to the high concentration of photogenerated carriers in the vicinity of the quantum dot/metal oxide interface, recombination at this interface may also play a role, as shown in Figure 1c (i). Studies of PbS QD/PCBM devices have identified interfacial recombination as an important loss mechanism, which can be faster than recombination in the bulk of the quantum dots.[30,31] Interfacial recombination has likewise been highlighted as an important process in quantum dot-sensitized solar cells, given the large interfacial area of these devices where a quantum dot sensitizer is coated onto a mesoporous metal oxide with a large surface area.[32] However, the extent of this interfacial recombination in quantum dot/metal oxide heterojunctions and its dependence on the properties of the constituent quantum dot and metal oxide layers are poorly understood.

The properties of metal oxides can be controlled through their synthesis conditions or by introducing external dopants.[18,33−37] Atmospheric atomic layer deposition (A-ALD), also known as spatial atomic layer deposition, is a fast, scalable technique that can be used to print conformal oxide coatings at low temperatures in atmospheric conditions, making it compatible with inexpensive substrates for low-cost photovoltaics (*e.g.*, roll-to-roll printing on plastics).[38,39] In contrast to conventional ALD, where precursors are sequentially cycled through a reaction chamber, A-ALD

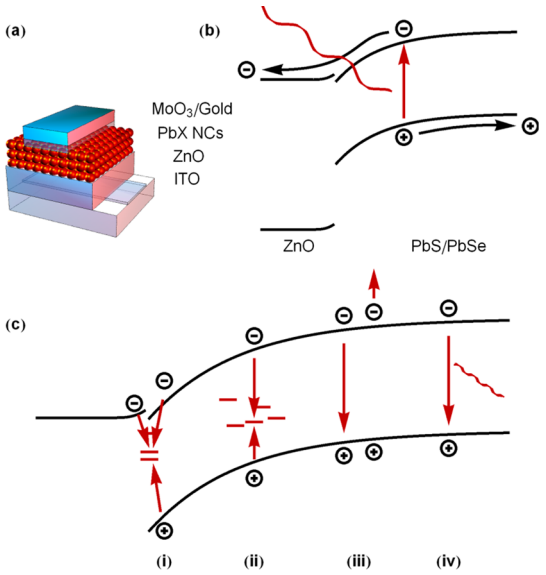

Figure 1. (a) Device structure and (b) working mechanism of a quantum dot/metal oxide solar cell. (c) Possible decay channels for photogenerated species in the PbS/PbSe quantum dots include (i) recombination *via* interfacial states, (ii) trap-assisted recombination, (iii) Auger recombination, and (iv) radiative decay.

moves a sample under alternating flows of precursor gases. A manifold head is used to deliver laminar flows of the precursors, which are separated by flows of inert shielding gas. The ability to control the properties of oxides *via* doping is well established for ALD techniques through the simple addition of dopant precursors.[23,35,40−42] Nitrogen doping has been shown to reduce the carrier concentration of ZnO made by ALD by several orders of magnitude[23] and under certain conditions even results in p-type behavior.[35] The nitrogen is believed to introduce an acceptor level *via* substitution on oxygen lattice sites, compensating the intrinsic donors.[43]

Here, we combine N:ZnO with PbSe and PbS quantum dots, which are well suited to form a depleted heterojunction solar cell with ZnO. The electronic properties of the quantum dots are determined largely by their size and surface characteristics. The size determines the band gap of the quantum dots, and the surface is believed to act as a source of electronic states within the band gap that prohibit efficient charge transport and aid recombination.[6,44] Notably, a large fraction of the atoms in a quantum dot are exposed to a surface site, making this an important consideration. Characterization of the PbS and PbSe quantum dots produced here using a variety of techniques (photoemission spectroscopy, transient photovoltage decay, transient absorption, as well as light and dark *IV* scans of operating solar cells) indicates a greater concentration of intragap states in the PbS quantum dots as compared to the PbSe quantum dots.

In this work, we probe the interfacial recombination process in PbX (X = S,Se) QD/ZnO solar cells by (i) varying

the nitrogen doping of A-ALD ZnO and (ii) studying both PbS and PbSe model systems. This allows us to study the effect of (i) the carrier concentration of the ZnO layer and (ii) the density of intragap states in the PbX layer. Interfacial recombination is found to be prevalent in devices where the quantum dot layer possesses a significant quantity of intragap states and the electron concentration in the adjacent oxide layer is high. However, we show that the recombination can be limited by appropriate tuning of the metal oxide properties.

RESULTS AND DISCUSSION

i. Solar Cell Performance. We deposited ZnO films using an A-ALD system with diethyl zinc as the zinc precursor and water as the oxygen source. Varying quantities of ammonia (NH_3) were added to the water to introduce different amounts of nitrogen dopant. Throughout this work, the amount of nitrogen dopant is quantified by the concentration of the ammonia solution used, *e.g.*, N:ZnO (33% NH_3) corresponds to a N:ZnO film made using a 33% NH_3 in H_2O solution, the highest dopant concentration used in this study. X-ray photoemission spectroscopy (XPS) data, presented in Section S1 of the Supporting Information, indicate that we successfully incorporated nitrogen into the oxygen lattice sites, resulting in a bulk doping level of up to 0.22 ± 0.04 atomic percent. The ZnO was verified to be polycrystalline wurtzite ZnO by X-ray diffraction (XRD), as shown in Figure S2 of the Supporting Information. Scanning electron microscopy revealed smooth, continuous films, with grain sizes on the order of 10−50 nm for a film approximately 250 nm thick, consistent with that reported previously for films made in a similar manner.[35]

For device fabrication, ZnO was deposited on ITO/glass substrates followed by a PbX quantum dot layer approximately 150 nm thick and a MoO_3/Au contact. The PbS and PbSe quantum dots with band gaps of approximately 1.3 and 1.02 eV, respectively, were synthesized as detailed in the Methods section. Figure 2 shows the current−voltage characteristics of the PbSe/ZnO and PbS/ZnO solar cells with a 200 nm ZnO layer and a variety of nitrogen doping levels. The performance of the PbSe solar cells exceeds that of the PbS cells due to a superior photocurrent. The power conversion efficiency of our PbSe solar cells approached 3% under simulated AM1.5G illumination, while the efficiency of the PbS solar cells varied between 0.8% for the undoped ZnO and 1.5% for the maximum doping level (33% NH_3). A striking difference in the dependence of device performance on nitrogen doping level is observed for the two systems. While the open-circuit voltage (V_{OC}) of the PbSe solar cells remains constant over the entire range of ZnO carrier concentrations studied, it increases dramatically with increasing doping level (lower carrier concentration) for the PbS solar cells (see Figure 3).

We note that the open-circuit voltages for the PbSe solar cells were slightly lower than the highest voltages of the PbS solar cells because the quantum dot band gap was smaller (1.02 eV for PbSe *vs* 1.3 eV for PbS). The open-circuit voltage is expected to scale with the quantum dot band gap, as observed for similar solar cells.[9,45] We observed the beneficial effect of ZnO doping on the V_{OC} of PbS solar cells with ZnO layers as thin as ∼50 nm (see Supplementary Figure S9), consistent with dense, homogeneous ZnO films.

Resistivity, Hall effect, and ultraviolet photoemission spectroscopy (UPS) studies (detailed in Section S1 of the Supporting Information) indicated that the main effect of nitrogen doping is a reduction in the carrier concentration from $\sim 10^{19}$ cm^{-3} in the undoped ZnO to $\sim 10^{17}$ cm^{-3} in the N:ZnO (33% NH_3). Thus the open-circuit voltage of the PbS solar cells increased by more than 50% when the ZnO carrier concentration was reduced by 2 orders of magnitude. The open-circuit voltage of a solar cell is the voltage at which recombination current equals photocurrent. The short-circuit photocurrent of both the PbSe and PbS devices was

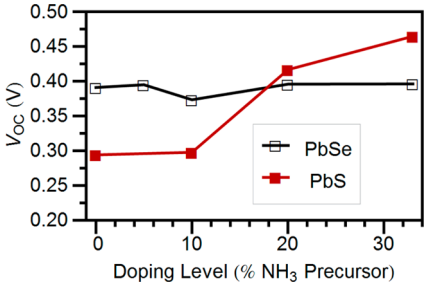

Figure 3. Open-circuit voltage as a function of nitrogen-doping precursor fraction.

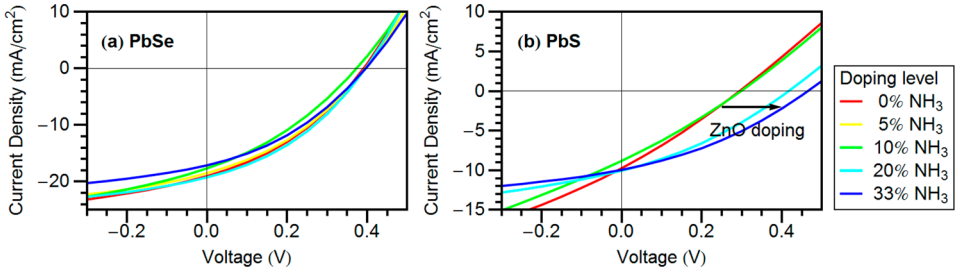

Figure 2. Current−voltage characteristics of solar cells with (a) PbSe and (b) PbS quantum dots and ZnO doped with various quantities of nitrogen precursor.

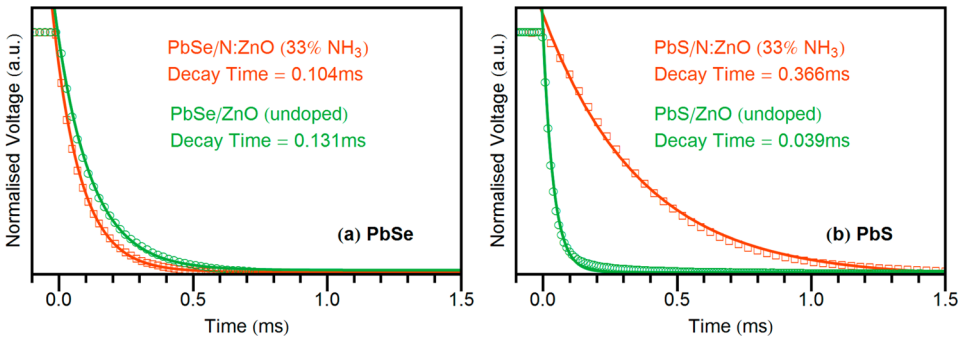

Figure 4. Photovoltage decay measurements on undoped and nitrogen-doped (a) PbSe and (b) PbS solar cells. The solid lines show monoexponential fits to the data with the time constant displayed in the inset.

relatively unchanged by nitrogen doping of the ZnO, suggesting that the increase in V_{OC} of the PbS/N:ZnO solar cells results from a reduction in the effective rate constant for recombination. This dependence of V_{OC} on the properties of the ZnO layer in the PbS cells strongly suggests that an interfacial recombination process is prevalent. In comparison, the PbSe devices appear insensitive to ZnO doping, indicating that a bulk mechanism may be the dominant recombination channel and the interface less important.

To investigate the difference between our PbS and PbSe systems, we examined their XPS, UPS, and infrared absorption spectra as well as mobility values derived by dark current measurements of devices operated in the space-charge-limited regime (see Supplementary Section S2). These measurements indicated that the two materials differ electronically as well as optically, and we find a significantly higher concentration of intragap states in our PbS quantum dots. The diminished role of interfacial recombination that we observed here for the PbSe devices, which are characterized by a cleaner band gap, would therefore suggest that intragap states play a crucial role in interfacial recombination in colloidal quantum dot solar cells. In the remainder of this study, we examine interfacial recombination in these devices and the cause of the distinctly different behavior in the PbS and PbSe systems.

ii. Transient Photovoltage Studies. Measurement of the transient photovoltage decay provides a way of directly probing the recombination in a solar cell. Upon illumination at open circuit, a voltage is produced across the device. When the light is switched off, charges recombine, resulting in a decay of the photovoltage. A fast decay of the voltage corresponds to fast recombination. We performed transient photovoltage measurements without background illumination, in order to probe specifically at low carrier densities, where the effect of any intragap states should be most pronounced. The intensity of the light-emitting diode was controlled such that the photovoltage was between 0.1 and 0.2 V so that a subset of the states within the band gap is probed.

Figure 4 shows the photovoltage decay of PbSe and PbS solar cells with undoped ZnO and N:ZnO (33% NH_3). We find that when undoped ZnO is used, recombination is more significant in the PbS cells (photovoltage decay is about 3 times faster than in the PbSe cell with undoped ZnO). This is in agreement with the low V_{OC} measured for PbS/ZnO. However, we find that doping the ZnO to reduce its free electron concentration results in a 10-fold increase in decay time for the PbS devices. As the same batch of PbS quantum dots was used, this dramatic change in decay kinetics cannot be attributed to recombination in the bulk of the quantum dot layer. Instead it provides direct evidence that the improved V_{OC} we observed in the PbS cells follows directly from a reduction in interfacial recombination due to doping of the ZnO (to reduce its carrier concentration).

Furthermore, the clear dependence of the recombination rate on the ZnO carrier concentration suggests that the supply of holes to the interface for recombination is reasonably fast in the PbS cells. If hole transport to recombination centers was the limiting factor, we would not expect the recombination time to vary with electron concentration. This hole transport occurs despite the expected presence of an opposing internal field, as shown in Figure 1b. Nagpal *et al.* showed that intragap states can result in non-band-like transport in thin films of quantum dots,[44] such that it is possible that the higher concentration of intragap states observed in our PbS quantum dots mediates the tunneling of holes to (or the trapping of holes at) the interface for recombination. In contrast, the decay time is independent of ZnO doping (within experimental error) for the PbSe solar cells. This suggests that the low density of intragap states in the PbSe quantum dots might limit the transport and capture of holes at the interface. As a result, the interfacial recombination is independent of the electron concentration and negligible compared to bulk processes.

We hence conclude at this stage that interfacial recombination in the PbS/ZnO solar cells is mediated by a comparatively large hole recombination current, such that the recombination rate can be limited by

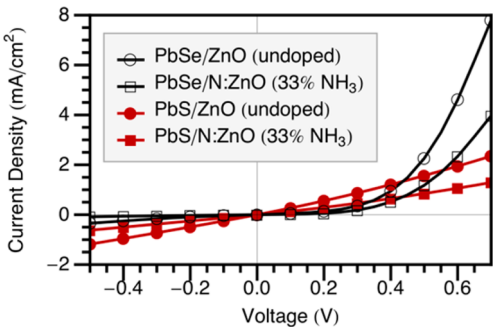

Figure 5. Dark current of PbS and PbSe solar cells.

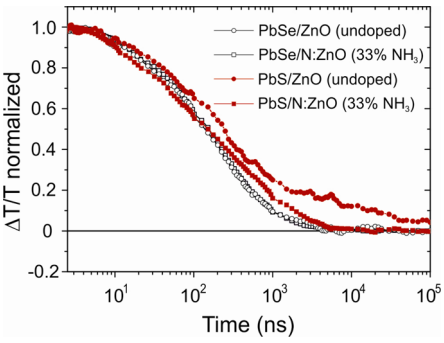

Figure 6. Transient absorption ground-state bleach (GSB) of PbSe and PbS devices with undoped ZnO and N:ZnO (33% NH_3).

controlling the density of electrons available for recombination. In contrast, the PbSe/ZnO solar cells show a lower recombination rate that is independent of electron concentration and thus is likely limited by hole transport to the interface and determined by bulk properties. To find out more about recombination currents in these solar cells, we investigated the dark currents in our devices.

iii. Dark Current. The dark current can give further clues about recombination in our devices, as we expect the dark current in a heterojunction to be dominated by recombination at the heterointerface. As seen in Figure 5, both the PbSe and PbS devices showed a decrease in overall dark current upon doping. This decrease can be attributed in part to the lower carrier concentration of the N:ZnO, which decreases the conductivity of the oxide. Reducing the carrier concentration of the ZnO is also expected to increase the built-in potential in the ZnO, which may inhibit the flow of electrons to the interface for recombination. Band diagrams of our devices were simulated using PC1D software[46] (see Figure S8a in the Supporting Information) and confirmed that an increased built-in potential is expected in the ZnO for the doping levels considered here. The dark currents of the PbS solar cells show an almost ohmic behavior in forward and reverse bias, indicating a negligible barrier for charge carriers to recombine. This effect can be seen in both doped and undoped ZnO/PbS solar cells. Upon illumination, our PbS cells change from an ohmic profile to a more diode-like behavior (see Figure 2b). Previous experiments by Nagpal *et al*. on optical field effect transistors (OFETs) indicated that conduction in quantum dot films in the dark is mainly due to intragap states, while it becomes more band-like upon illumination.[44] Thus the ohmic characteristic observed here for our PbS/ZnO devices is consistent with our assertion of a higher density of intragap states in the PbS quantum dots. Furthermore, the ohmic nature of the dark current demonstrates that the intragap states facilitate the tunneling of holes to the interface for recombination, despite the presence of an opposing built-in potential. This is consistent with our transient photovoltage measurements on PbS/ZnO, where the dependence of recombination rate on the ZnO electron concentration indicated a comparatively fast hole capture rate (see Figure 4b). While the work of Naghpal *et al*. indicates that the extent of this intragap transport will be reduced under illumination, the current characteristic of the PbS/ZnO device under illumination (Figure 2b) is still far from that of an ideal diode, suggesting that some intragap behavior remains.

In contrast, we observed diode behavior in both the light and dark for our solar cells based on PbSe quantum dots, consistent with a low intragap state density. We hence expect that hole transport to the interface is inhibited and that residual interfacial recombination is likely overshadowed by other recombination mechanisms present in the bulk of the quantum dot film. In agreement with Ip *et al*. we attribute the better device performance of the PbSe solar cells to a lower intragap state density.[6]

iv. Transient Absorption. We have established that the increased V_{OC} in our PbS/N:ZnO solar cells is due to reduced interfacial recombination that is mediated by intragap states in the quantum dots. We now use transient absorption (TA) spectroscopy to examine how the doping of ZnO with nitrogen suppresses this interfacial recombination. TA spectroscopy uses a narrow band pump beam to create a population of excited states at time $t = t_0$. At some later time $t = t_0 + \Delta t$, a broadband beam is used to probe the system and the transmission T_1 is recorded. The differential transmission $\Delta T/T = (T_1 - T_0)/T_0$ is then calculated, where T_0 is the transmission of the unperturbed system. Since the pump beam promotes species from the ground state to higher lying excited states, the magnitude of the absorption of the ground state is reduced (*i.e.*, transmission is increased), yielding a positive $\Delta T/T$ signal known as the ground-state bleach (GSB).

Here we performed long-time (1 ns to 0.1 ms) TA measurements on the PbS and PbSe devices at short circuit with both undoped ZnO and N:ZnO (33% NH_3). Samples were excited at 532 nm (20 nm pulsewidth) and probed in the near IR (800−1650 nm). Figure 6 shows the kinetics of the GSB of our devices. The decay of the GSB (repopulation of the ground state)

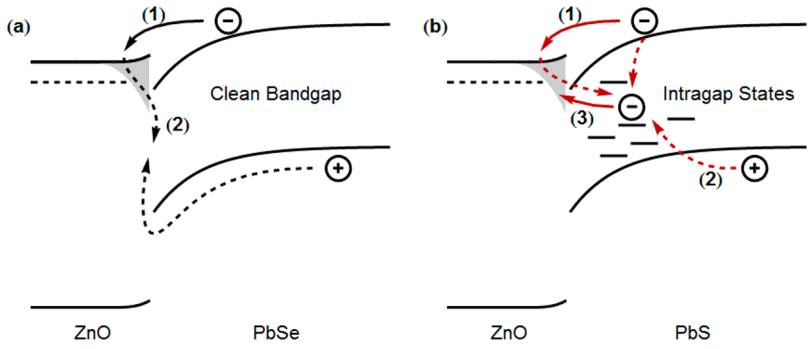

Figure 7. Proposed interfacial recombination mechanism of PbX/ZnO solar cells. (a) Cells with PbSe quantum dots exhibit efficient electron collection from the PbSe conduction band by the oxide (1) and limited interfacial recombination (2). (b) PbS quantum dots exhibit an increased density of intragap states that increase the interfacial recombination of photogenerated electrons by facilitating hole transport to the interface (2) and trapping electrons from the conduction band of the quantum dots or adjacent ZnO. When the ZnO is doped to reduce its carrier concentration, the back-transfer of electrons from the ZnO is reduced and/or some of the trapped carriers can be recovered by injection into sub-band-gap states of the ZnO (3).

corresponds to the successful collection of photogenerated charges or their recombination within the device. Doping of the ZnO is expected to have little influence on hole collection from the PbS and PbSe layers, such that we can attribute differences in our GSB signals to electrons present in the quantum dots.

The PbSe devices with undoped ZnO and N:ZnO (33% NH_3) exhibit almost identical decay kinetics over the whole range of 1 ns to 0.1 ms, indicating that photogenerated charge collection and recombination processes are unaffected by the ZnO carrier concentration. In the PbS devices on the other hand, a clear difference in decay kinetics is observed when the ZnO is doped with nitrogen to reduce its carrier concentration. For times longer than 1 μs, a long-lived tail is observed for the PbS/ZnO device, which suggests that electrons accumulate in the PbS layer when undoped ZnO is used. These could be photoexcited electrons that are generated in the quantum dots and accumulate at the PbS/ZnO interface or electrons from the ZnO that back-transfer into the PbS. In contrast, the PbS/N:ZnO (33% NH_3) device shows no long-lived signal. This indicates that electron collection from the PbS by the oxide is improved and/or back-transfer of electrons from the oxide to the PbS is limited by doping the ZnO to reduce the occupancy of its electronic states, either of which would reduce the amount of interfacial recombination.

Given that the conduction band edges are similarly positioned for our PbS and PbSe (see Figure S8 in the Supporting Information) and similar couplings between the PbX quantum dots and ZnO are expected, we would anticipate that electron transfer from the conduction band of the PbS quantum dots would be similarly efficient to the ZnO and N:ZnO (33% NH_3), as was the case for the PbSe quantum dots. The long-lived GSB signal in the PbS/ZnO device therefore suggests that the measured electrons do not reside exclusively in the conduction band of the PbS. Instead, some electrons in the PbS layer likely accumulate at the trap states within the band gap of the PbS quantum dots. Interestingly, the decay of the GSB signals for the PbS/ZnO and PbS/N:ZnO (33% NH_3) devices between 20 ns and 20 μs is similar, with the exception of a constant offset (a larger $\Delta T/T$ at all times for the undoped ZnO). This suggests that in the PbS/ZnO device the additional species of long-lived "trapped" charges are created within the first 20 ns, and then between 20 ns and 20 μs the extraction and recombination rates for "free charges" are the same as in the PbS/N:ZnO (33% NH_3) device.

On the basis of the measurements presented thus far we propose an interfacial recombination mechanism as illustrated in Figure 7. In the PbSe devices, the absence of a high density of intragap states means that most photogenerated electrons in the quantum dot layer near the interface are located in the PbSe conduction band and are injected into the conduction band of the oxide, as shown in process 1 of Figure 7a. A sufficient quantity of vacant electron states is present in the ZnO such that electron collection from the PbSe is efficient and doping the oxide to reduce its concentration of free electrons does not significantly influence charge collection kinetics. In the absence of a significant quantity of intragap states and the presence of a built-in field that inhibits hole transport to the interface, interfacial recombination (process 2 of Figure 7a) is limited and bulk recombination mechanisms may dominate.

In the PbS devices on the other hand, electrons accumulate near the interface in the large density of intragap states (within 20 ns of illumination). The accumulated electrons may originate from the quantum dot layer (photogenerated electrons) or from the adjacent ZnO (back-transfer of electrons), as illustrated in Figure 7b. The simulations presented in Figure S8b of the Supporting Information indicate that a high electron density is expected at the surface of the undoped oxide. If not removed, these electrons accumulated in the PbS intragap states are liable to recombine with holes in the quantum dots. Notably, the intragap states facilitate the transport of holes to the interface for

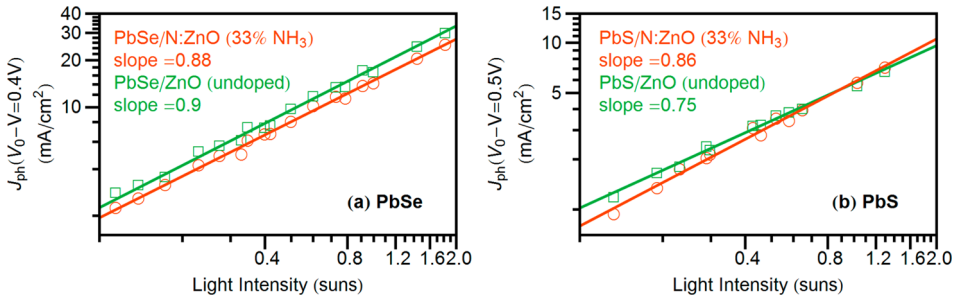

Figure 8. Light-intensity-dependent photocurrent for (a) PbSe and (b) PbS solar cells.

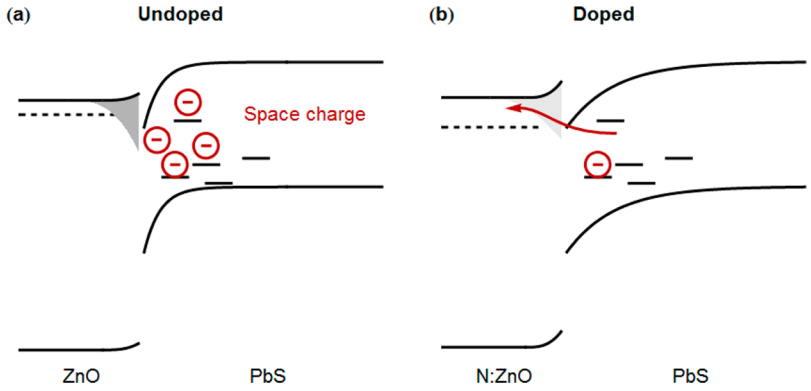

Figure 9. Band diagram of the effect of doping the ZnO on PbS QD/ZnO devices. (a) Space charge builds up near the interface in solar cells with undoped ZnO, limiting the device performance. (b) Doping the ZnO results in more efficient electron collection and/or reduced back-transfer of electrons from ZnO, suppressing electron population in the intragap states.

recombination, as indicated by transient photovoltage and dark current measurements (process 2 in Figure 7b). Accumulated electrons may be collected by being re-excited to the PbS conduction band, then transferring into the ZnO conduction band, in a manner similar to the PbSe devices (process 1 in Figure 7b). Alternatively, since metal oxides are known to have a significant density of sub-band-gap surface states,[47,48] the presence of such states in the ZnO may facilitate the collection of accumulated electrons directly from the PbS intragap sites, as shown in process 3 of Figure 7b. In this process, the charge transfer rate is expected to depend on the density of accepting states.[49,50] Doping the ZnO will significantly reduce the occupancy of its mobile electronic states near its surface, *e.g.*, from a population of more than 10^{16} cm^{-3} at a depth of 2 nm from the interface for the ZnO with a bulk concentration of 10^{19} cm^{-3} to less than 10^{10} cm^{-3} for the N:ZnO with a bulk carrier concentration of 10^{17} cm^{-3} (as determined by our simulations in Figure S8b of the Supporting Information). This provides a greater density of accepting states for electron transfer. Therefore, by doping the ZnO to reduce its carrier concentration by 2 orders of magnitude, we prevented the back-transfer of electrons to intragap states in the PbS quantum dots and/or enabled faster charge transfer from intragap states in the PbS quantum dots to sub-band-gap states in the oxide.

v. Intensity-Dependent Measurements. Finally, to verify the interfacial recombination mechanism outlined in Figure 7, intensity-dependent measurements were performed to characterize the accumulation of electrons at the metal oxide/quantum dot interface. In a photovoltaic device where the transport and removal of the electrons and holes are unbalanced, space charge is known to build up within the device. As noted by Goodman and Rose,[51] this space charge places a fundamental limit on the achievable current output, as the photogenerated current can reach a maximum electrostatically allowed value. Light-intensity-dependent measurements of the photocurrent of a solar cell allow identification of whether a solar cell current is space-charge limited.[51,52] If the space charge does not limit the overall current, the photocurrent scales linearly with light intensity. When the photogenerated current exceeds the electrostatically allowed current and thus will be limited by the space charge, the current then scales with light intensity to the power 3/4. Hence the two regimes can be distinguished by their dependence on light intensity.

Figure 8 shows the photocurrent J_{ph} (difference between light and dark current) as a function of light intensity for the PbSe (a) and PbS (b) devices, with undoped ZnO and N:ZnO (33% NH_3). The photocurrent is shown for effective applied voltages (defined as $V_0 - V$ with $J_{ph}(V_0) = 0$) of 0.4 and 0.5 V for PbSe and PbS, respectively. For these $V_0 - V$, the photocurrents show a square-root dependence on voltage for all intensities considered (see Supplementary Figure S10). It is in this

square-root voltage dependence regime that any space-charge effects are expected to be visible.[54]

We see in Figure 8a that the photocurrent of the PbSe solar cells scales with light intensity at a slope reasonably close to unity, regardless of the ZnO doping level. For the PbS system (Figure 8b), the cells with undoped ZnO show a slope of 3/4, indicating that they are space-charge limited, which results in increased recombination. Nitrogen doping of the ZnO increases this slope to a value more similar to that in the PbSe devices. The fact that the space-charge-limited regime is reached for PbS on ZnO but not for PbS on N:ZnO (33% NH_3) provides additional evidence that electrons accumulate in the PbS at the interface with undoped ZnO (see Figure 9). As discussed in Section S1.iii of the Supporting Information, the carrier mobility in our ZnO is reduced by less than an order of magnitude with nitrogen doping, such that the avoidance of the space-charge limit is unlikely to be attributable to more balanced charge transport and is instead due to different electron collection efficiencies from the PbS. To further support this conclusion, we prepared solar cells using ZnO films that were synthesized at lower temperatures, for which a lower electron mobility within the ZnO is expected (identical PbS quantum dots were used). Those solar cells did not show the increased V_{OC} we saw upon doping, suggesting that unbalanced charge removal from the PbS, rather than unbalanced charge transport through the device, is responsible for the accumulation of space charge.

Figure 9 demonstrates the accumulation of space charge in the PbS devices. In the PbS QD/ZnO devices (Figure 9a), the back-transfer of electrons to the PbS intragap states and/or poor collection from these states results in the buildup of a larger space charge in the PbS QD near the interface than in the PbS/N:ZnO devices (Figure 9b). This space charge alters the steady-state electric-field distribution in the device, concentrating it near the PbS/ZnO interface in such a way as to enhance the collection of trapped electrons. This reduces the width of the collection region and the electrostatically allowed current, thus limiting the achievable photocurrent.

CONCLUSIONS

In this study we examined the influence of (i) the carrier concentration of the ZnO layer and (ii) the density of quantum dot intragap states on interfacial recombination in PbX (X = S,Se) quantum dot/ZnO solar cells. ZnO films were synthesized using a scalable A-ALD technique and doped with nitrogen to vary the carrier concentration by 2 orders of magnitude. Characterization by XPS, UPS, IR absorption, and transport measurements indicated a greater density of intragap states in our PbS quantum dots than the PbSe dots. A general picture for interfacial recombination in PbX/ZnO quantum dot solar cells was presented in Figure 7, which is consistent with results from transient photovoltage, dark current, transient absorption, and light-intensity-dependent photocurrent characterization. Intragap states in the quantum dots trap electrons near the quantum dot/metal oxide interface and facilitate the transport of holes to the interface for recombination with the trapped electrons. The trapped electrons may originate from absorption within the QD layer and/or may be back-transferred from the ZnO. In the presence of a significant density of intragap QD states, this recombination may be limited by reducing the ZnO carrier concentration to prevent the back-transfer of electrons and/or enable the collection of trapped electrons *via* sub-bandgap states in the ZnO. This model is also consistent with the device characterization performed in this work. The performance of our PbSe cells (few intragap states) was independent of the carrier concentration in the ZnO, with a constant V_{OC} around 0.4 V and power conversion efficiency approaching 3%. The efficiency of the PbS cells (high density of intragap states) on the other hand increased from 0.8% to 1.5% (V_{OC} increased from <0.3 V to >0.45 V) as the ZnO carrier concentration was reduced by nitrogen doping. Our study demonstrates the nature of interfacial recombination in quantum dot/metal oxide solar cells and stresses the importance of controlling the properties of the quantum dots and metal oxide. Namely, the synthesis of quantum dots with clean band gaps is desirable, and the ability to control the electrical properties of the metal oxide, in addition to the energetic position of its conduction band edge, is important in systems prone to interfacial recombination. We have demonstrated that nitrogen doping is an efficient technique to achieve this control and can be used to improve the efficiency of scalable quantum dot/metal oxide solar cells.

METHODS

Quantum Dot Synthesis. All chemicals are purchased from Sigma Aldrich if not stated otherwise and were anhydrous if available. PbS quantum dots were synthesized according to an existing synthesis procedure reported previously.[53] In a typical synthesis lead oxide (0.47 g, 2.1 mmol, 99.99%) and oleic acid (11 mL, 35 mmol, technical grade, 90%, OA) in 1-octadecene (25 mL, technical grade, 90%, ODE) are degassed at 100 °C under vacuum for 3 h. Upon lead oleate formation the solution is set under nitrogen and heated to 130 °C. Separately, the sulfur precursor bis(trimethylsilyl) sulfide (210 μL, 1 mmol, synthesis grade, TMS) in ODE (4 mL, anhydrous) is prepared under inert atmosphere and rapidly injected into the degassed Pb-oleate solution. Upon injection the solution is slowly cooled to room temperature by removing the heating mantle. The quantum dots formed are flocculated by addition of an ethanol/hexane mixture, washed twice using the same solvents, and stored in octane under a nitrogen atmosphere.

The synthesis of PbSe quantum dots follows previous work.[45] In summary, lead diacetate trihydrate (1.3 g, 3.4 mmol,

trace metal basis, 99.999%) is degassed with OA (2.1 mL, 7.6 mmol, technical grade, 90%) in ODE (19 mL, technical grade, 90%) at 80 °C under vacuum for 2 h. Under inert atmosphere, the solution is then heated to 160 °C and the Se precursor solution, consisting of Se (0.85 g, 10.8 mmol, 325 mesh, 99.999%, Alpha Aeser) and diphenyl phosphine (26.1 μL, 15 μmol, 98%) in tri-*n*-octylphosphine (10.8 mL, 24.2 mmol, 97%), is injected rapidly. After 1.5 min the reaction is quenched by placing the flask into a water bath. The formed PbSe quantum dots are separated from the reaction solution by flocculating with an *n*-butanol/methanol mixture in a nitrogen-filled glovebox. Hexane, *n*-butanol, and methanol are used for two additional cleaning steps. Finally, the quantum dots are dispersed in octane and stored under nitrogen.

The PbS and PbSe quantum dot absorption spectrum is shown in Supplementary Figure S4.

ZnO Synthesis. ZnO films were deposited on ITO/glass substrates at 150 °C using an A-ALD system operated under chemical vapor deposition conditions. The substrates were sonicated in acetone and 2-propanol, then placed in a UV/ozone cleaner for 10 min prior to deposition. Diethyl zinc was used as the zinc source and water as the oxygen source. Varying amounts of ammonia were added to the water to control the level of nitrogen doping. Nitrogen was used as the inert gas to bubble the precursors, carry the precursors to the substrate, and shield the adjacent precursor flows. The ITO/glass substrates were passed underneath the precursor flows at a distance of approximately 60 μm and speed of 50 mm/s. From 120 to 2400 zinc−water cycles were employed to deposit films of varying thickness. Thickness measurements with a Dektak Profilometer indicated a deposition rate of approximately 0.16 nm per cycle. Following deposition, all films were annealed for 1 h at 350 °C on a hot plate in air.

Materials Characterizaton. *X-ray Diffraction.* Measurements were performed using a Bruker D8 theta/theta XRD system with Cu Kα radiation (λ = 0.15418 nm) and a LynxEye position-sensitive detector. Scanning electron micrographs were obtained using a LEO VP-1530 field emission SEM.

Photoemission Spectroscopy. The PES samples were transferred to the ultrahigh-vacuum chamber (ESCALAB 250Xi) for UPS/XPS measurements. UPS measurements were performed using a double-differentially pumped He gas discharge lamp emitting He I radiation ($h\nu$ = 21.22 eV) with a pass energy of 2 eV. The low-energy edge of the valence band is used to determine the ionization potential of the measured film.[54] XPS measurements were carried out using an XR6 monochromated Al Kα X-ray source ($h\nu$ = 1486.6 eV) with a 650 μm spot size. Ar^+ ion gun etching was performed using an ion energy of 3000 eV.

Absorption Measurements. Films were spin-cast on Spectrosil quartz glass substrates. The spectra were collected using a Hewlett-Packard HP 8453 UV−vis spectrometer and a PerkinElmer Lambda 9 UV−vis−IR spectrometer for infrared absorption.

Resistivity and Hall Effect Measurements. Films of 1 cm^2 were deposited on borosilicate glass and examined in a van der Pauw geometry with Al−In contacts. A Keithley 6221 current source, a Keithley 182 nanovoltmeter, and a home-built differential electrometer with an input resistance of 10^{14} Ω were employed.

Device Fabrication. To fabricate solar cells, ZnO films were deposited on prepatterned ITO slides as described above. They were transferred to a nitrogen-filled glovebox, and quantum dots (15−35 mg/mL in octane) were deposited by a layer-by-layer technique. A thin layer of quantum dots was spin-cast on the ZnO films followed by dropping 1,3-benzenedithiol (BDT) in acetonitrile (0.02 M) on the film to cross-link the quantum dots. Three seconds after BDT deposition the liquid was spun off followed by spinning cycles with pure acetonitrile and pure octane. This was repeated until the desired thickness (150 nm) was reached. Molybdenum trioxide (7 nm) and 80 nm gold were deposited as the top contact. As a control study, a subset of the solar cells was fabricated without the molybdenum trioxide interlayer, and we find the same relative differences in device operation between PbS and PbSe and between doped and undoped ZnO, although the overall device performance is worse.

Device Characterization. *Current−Voltage Characterization.* Measurements were taken using a Keithley 2636A source-measure unit in the dark and under an Oriel 92250A solar simulator, corrected for spectral mismatch. Light-intensity-dependent measurements were taken under the same solar simulator with a series of attenuators (23−100%) and by changing the light level of the solar simulator (0.5 sun to 2 sun).

External Quantum Efficiency. We measured the photoresponse as a function of photon energy using light from an Oriel Cornerstone 260 monochromator. External quantum efficiencies were calculated from this, comparing the solar cell photoresponse to the response from a reference diode.

Photovoltage Decay. Measurements were carried out using a green (525 nm) light-emitting diode connected to a Hewlett-Packard 8116A pulse/function generator producing a 100 ms square voltage pulse. The voltage response from the solar cell was recorded using an Agilent DSO6052A digitalizing oscilloscope (input impedance 1 MΩ). Measurements were taken without background-light bias. We also performed measurements with a 1 sun background illumination; however the RC constant of our measurement setup was too slow to resolve the faster dynamics under those conditions.

Transient Absorption. The PbS device kinetics of the GSB were measured between 910 and 970 nm at a pump fluence of 10 $\mu J/cm^2$, which is in the linear regime. The kinetics of the GSB of PbSe devices were measured slightly more toward the red (1150 and 1300 nm) due to the lower band gap. Pump fluence was kept at 2.8 $\mu J/cm^2$. All kinetics were measured at a white-light bias of about 2% sun to simulate the UV doping of the ZnO occurring under operation conditions. The bias was chosen such that the total photocurrent is in the linear regime, *i.e.*, that the overall current is the sum of the contributions from pump and probe beam as well as the white-light bias.

Conflict of Interest: The authors declare no competing financial interest.

Supporting Information Available: Supporting Information outlining the material characterization, heterojunction simulations, and device characterization is available free of charge *via* the Internet at http://pubs.acs.org.

Acknowledgment. The authors thank Prof. Sir Richard Friend and Dr. Frank Schoofs for helpful discussions. B.E. acknowledges the EPSRC SUPERGEN Excitonic Solar Cells Consortium and the KACST-Cambridge Research Project. K.P.M. acknowledges Girton College (Cambridge). J.L.M.D. acknowledges the ERC Advanced Investigator Grant NOVOX ERC-2009-adG247276.

REFERENCES AND NOTES

1. Bhaumik, S.; Ghosh, B.; Pal, A. J. Color Tunable Light-Emitting Diodes Based on Copper Doped Semiconducting Nanocrystals. *Appl. Phys. Lett.* **2011**, *99*, 83106.
2. Talapin, D. V.; Murray, C. B. PbSe Nanocrystal Solids for N- and P-Channel Thin Film Field-Effect Transistors. *Science* **2005**, *310*, 86.
3. Sukhovatkin, V.; Hinds, S.; Brzozowski, L.; Sargent, E. H. Colloidal Quantum-Dot Photodetectors Exploiting Multiexciton Generation. *Science* **2009**, *324*, 1542–1544.
4. Konstantatos, G.; Howard, I.; Fischer, A.; Hoogland, S.; Clifford, J.; Klem, E.; Levina, L.; Sargent, E. H. Ultrasensitive Solution-Cast Quantum Dot Photodetectors. *Nature* **2006**, *442*, 180–183.
5. Tang, J.; Sargent, E. H. Infrared Colloidal Quantum Dots for Photovoltaics: Fundamentals and Recent Progress. *Adv. Mater.* **2011**, *23*, 12–29.
6. Ip, A. H.; Thon, S. M.; Hoogland, S.; Voznyy, O.; Zhitomirsky, D.; Debnath, R.; Levina, L.; Rollny, L. R.; Carey, G. H.; Fischer, A.; *et al.* Hybrid Passivated Colloidal Quantum Dot Solids. *Nat. Nanotechnol.* **2012**, *7*, 1–6.
7. Pattantyus-Abraham, A. G.; Kramer, I. J.; Barkhouse, D. A. R.; Wang, X.; Konstantatos, G.; Debnath, R.; Levina, L.; Raabe, I.; Nazeeruddin, M. K.; Grätzel, M.; *et al.* Depleted-Heterojunction Colloidal Quantum Dot Solar Cells. *ACS Nano* **2010**, *4*, 3374–3380.
8. Sargent, E. H. Colloidal Quantum Dot Solar Cells. *Nat. Photonics* **2012**, *6*, 133–135.

9. Gao, J.; Luther, J. M.; Semonin, O. E.; Ellingson, R. J.; Nozik, A. J.; Beard, M. C. Quantum Dot Size Dependent J-V Characteristics in Heterojunction ZnO/PbS Quantum Dot Solar Cells. *Nano Lett.* **2011**, *11*, 1002–1008.
10. Leschkies, K. S.; Beatty, T. J.; Kang, M. S.; Norris, D. J.; Aydil, E. S. Solar Cells Based on Junctions between Colloidal PbSe Nanocrystals and Thin ZnO Films. *ACS Nano* **2009**, *3*, 3638–3648.
11. Luther, J. M.; Gao, J.; Lloyd, M. T.; Semonin, O. E.; Beard, M. C.; Nozik, A. J. Stability Assessment on a 3% Bilayer PbS/ZnO Quantum Dot Heterojunction Solar Cell. *Adv. Mater.* **2010**, *22*, 3704–3707.
12. Semonin, O. E.; Luther, J. M.; Choi, S.; Chen, H.-Y.; Gao, J.; Nozik, A. J.; Beard, M. C. Peak External Photocurrent Quantum Efficiency Exceeding 100% *via* MEG in a Quantum Dot Solar Cell. *Science* **2011**, *334*, 1530–1533.
13. Yu, D.; Wang, C.; Guyot-Sionnest, P. n-Type Conducting CdSe Nanocrystal Solids. *Science* **2003**, *300*, 1277.
14. Ma, W.; Luther, J. M.; Zheng, H.; Wu, Y.; Alivisatos, A. P. Photovoltaic Devices Employing Ternary PbS_xSe_{1-x} Nanocrystals. *Nano Lett.* **2009**, *9*, 1699–1703.
15. Jeong, K. S.; Tang, J.; Liu, H.; Kim, J.; Schaefer, A. W.; Kemp, K. W.; Levina, L.; Wang, X.; Hoogland, S.; Debnath, R.; *et al*. Enhanced Mobility-Lifetime Products in PbS Colloidal Quantum Dot Photovoltaics. *ACS Nano* **2011**.
16. Barkhouse, D. A. R.; Debnath, R.; Kramer, I. J.; Zhitomirsky, D.; Pattantyus-Abraham, A. G.; Levina, L.; Etgar, L.; Grätzel, M.; Sargent, E. H. Depleted Bulk Heterojunction Colloidal Quantum Dot Photovoltaics. *Adv. Mater.* **2011**, *23*, 3134–3138.
17. Kramer, I. J.; Zhitomirsky, D.; Bass, J. D.; Rice, P. M.; Topuria, T.; Krupp, L.; Thon, S. M.; Ip, A. H.; Debnath, R.; Kim, H.-C.; *et al*. Ordered Nanopillar Structured Electrodes for Depleted Bulk Heterojunction Colloidal Quantum Dot Solar Cells. *Adv. Mater.* **2012**, *24*, 2315–2319.
18. Liu, H.; Tang, J.; Kramer, I. J.; Debnath, R.; Koleilat, G. I.; Wang, X.; Fisher, A.; Li, R.; Brzozowski, L.; Levina, L.; *et al*. Electron Acceptor Materials Engineering in Colloidal Quantum Dot Solar Cells. *Adv. Mater.* **2011**, *23*, 3832–3837.
19. Willis, S. M.; Cheng, C.; Assender, H. E.; Watt, A. A. R. The Transitional Heterojunction Behavior of PbS/ZnO Colloidal Quantum Dot Solar Cells. *Nano Lett.* **2012**, *12*, 1522–1526.
20. Wang, R. Y.; Feser, J. P.; Lee, J.-S.; Talapin, D. V.; Segalman, R.; Majumdar, A. Enhanced Thermopower in PbSe Nanocrystal Quantum Dot Superlattices. *Nano Lett.* **2008**, *8*, 2283–2288.
21. Luther, J. M.; Law, M.; Beard, M. C.; Song, Q.; Reese, M. O.; Ellingson, R. J.; Nozik, A. J. Schottky Solar Cells Based on Colloidal Nanocrystal Films. *Nano Lett.* **2008**, *8*, 3488–3492.
22. Pearton, S. J.; Abernathy, C. R.; Overberg, M. E.; Thaler, G. T.; Norton, D. P.; Theodoropoulou, N.; Hebard, a. F.; Park, Y. D.; Ren, F.; Kim, J.; *et al*. Wide Band Gap Ferromagnetic Semiconductors and Oxides. *J. Appl. Phys.* **2003**, *93*, 1.
23. Lim, S. J.; Kwon, S.-ju; Kim, H.; Park, J.-S. High Performance Thin Film Transistor with Low Temperature Atomic Layer Deposition Nitrogen-Doped ZnO. *Appl. Phys. Lett.* **2007**, *91*, 183517.
24. Hwang, Y. J.; Boukai, A.; Yang, P. High Density n-Si/n-TiO_2 Core/Shell Nanowire Arrays with Enhanced Photoactivity. *Nano Lett.* **2009**, *3*, 1–6.
25. Lakhwani, G.; Roijmans, R. F. H.; Kronemeijer, A. J.; Gilot, J.; Janssen, R. A. J.; Meskers, S. C. J. Probing Charge Carrier Density in a Layer of Photodoped ZnO Nanoparticles by Spectroscopic Ellipsometry. *J. Phys. Chem. C* **2010**, *114*, 14804–14810.
26. Schmidt-Mende, L.; MacManus-Driscoll, J. L. ZnO - Nanostructures, Defects, and Devices. *Mater. Today* **2007**, *10*, 40–48.
27. Wehrenberg, B. L.; Wang, C.; Guyot-Sionnest, P. Interband and Intraband Optical Studies of PbSe Colloidal Quantum Dots. *J. Phys. Chem. B* **2002**, *106*, 10634–10640.
28. Klimov, V. I.; Mikhailovsky, A. A.; McBranch, D. W.; Leatherdale, C. A.; Bawendi, M. G. Quantization of Multiparticle Auger Rates in Semiconductor Quantum Dots. *Science* **2000**, *287*, 1011–1013.
29. Patel, A. A.; Wu, F.; Zhang, J. Z.; Torres-Martinez, C. L.; Mehra, R. K.; Yang, Y.; Risbud, S. H. Synthesis, Optical Spectroscopy and Ultrafast Electron Dynamics of PbS Nanoparticles with Different Surface Capping. *J. Phys. Chem. B* **2000**, *104*, 11598–11605.
30. Zhao, N.; Osedach, T. P.; Chang, L.-Y.; Geyer, S. M.; Wanger, D.; Binda, M. T.; Arango, A. C.; Bawendi, M. G.; Bulovic, V. Colloidal PbS Quantum Dot Solar Cells with High Fill Factor. *ACS Nano* **2010**, *4*, 3743–3752.
31. Osedach, T. P.; Zhao, N.; Geyer, S. M.; Chang, L.-Y.; Wanger, D. D.; Arango, A. C.; Bawendi, M. G. C.; Bulović, V. Interfacial Recombination for Fast Operation of a Planar Organic/QD Infrared Photodetector. *Adv. Mater.* **2010**, *22*, 5250–5254.
32. Hetsch, F.; Xu, X.; Wang, H.; Kershaw, S. V.; Rogach, A. L. Semiconductor Nanocrystal Quantum Dots as Solar Cell Components and Photosensitizers: Material, Charge Transfer, and Separation Aspects of Some Device Topologies. *J. Phys. Chem. Lett.* **2011**, *2*, 1879–1887.
33. Nel, J.; Auret, F.; Wu, L.; Legodi, M.; Meyer, W.; Hayes, M. Fabrication and Characterisation of NiO/ZnO Structures. *Sens. Actuators B Chem.* **2004**, *100*, 270–276.
34. Lu, J. G.; Fujita, S.; Kawaharamura, T.; Nishinaka, H.; Kamada, Y.; Ohshima, T.; Ye, Z. Z.; Zeng, Y. J.; Zhang, Y. Z.; Zhu, L. P.; *et al*. Carrier Concentration Dependence of Band Gap Shift in N-Type ZnO:Al Films. *J. Appl. Phys.* **2007**, *101*, 083705.
35. Dunlop, L.; Kursumovic, A.; MacManus-Driscoll, J. L. Reproducible Growth of P-Type ZnO:N Using a Modified Atomic Layer Deposition Process Combined with Dark Annealing. *Appl. Phys. Lett.* **2008**, *93*, 172111–1721113.
36. Izaki, M.; Omi, T. Transparent Zinc Oxide Films Prepared by Electrochemical Reaction. *Appl. Phys. Lett.* **1996**, *68*, 2439.
37. Musselman, K. P.; Wisnet, A.; Iza, D. C.; Hesse, H. C.; Scheu, C.; MacManus-Driscoll, J. L.; Schmidt-Mende, L. Strong Efficiency Improvements in Ultra-Low-Cost Inorganic Nanowire Solar Cells. *Adv. Mater.* **2010**, *22*, E254–258.
38. Levy, D. H.; Nelson, S. F.; Freeman, D. Oxide Electronics by Spatial Atomic Layer Deposition. *J. Display Technol.* **2009**, *5*, 484–494.
39. Levy, D. H.; Freeman, D.; Nelson, S. F.; Cowdery-Corvan, P. J.; Irving, L. M. Stable ZnO Thin Film Transistors by Fast Open Air Atomic Layer Deposition. *Appl. Phys. Lett.* **2008**, *92*, 192101.
40. Lujala, V.; Skarp, J.; Tammenmaa, M.; Suntola, T. Atomic Layer Epitaxy Growth of Doped Zinc Oxide Thin Films from Organometals. *Appl. Surf. Sci.* **1994**, *82*, 34–40.
41. Pore, V.; Heikkil, M.; Ritala, M.; Leskel, M.; Areva, S. Atomic Layer Deposition of $TiO_{2-x}N_x$ Thin Films for Photocatalytic Applications. *J. Photochem. Photobiol. A* **2006**, *177*, 68–75.
42. Kim, S. K.; Choi, G.-J.; Lee, S. W. Y.; Seo, M.; Han, J. H.; Ahn, H.-S.; Han, S.; Hwang, C. S. Al-Doped TiO_2 Films with Ultralow Leakage Currents for Next Generation DRAM Capacitors. *Adv. Mater.* **2008**, *20*, 1429–1435.
43. Park, C. H.; Zhang, S. B.; Wei, S.-H. Origin of p-Type Doping Difficulty in ZnO: The Impurity Perspective. *Phys. Rev. B* **2002**, *66*, 73202.
44. Nagpal, P.; Klimov, V. I. Role of Mid-Gap States in Charge Transport and Photoconductivity in Semiconductor Nanocrystal Films. *Nat. Commun.* **2011**, *2*, 486.
45. Ehrler, B.; Walker, B. J.; Böhm, M. L.; Wilson, M. W. B. B.; Vaynzof, Y.; Friend, R. H.; Greenham, N. C. *In Situ* Measurement of Exciton Energy in Hybrid Singlet-Fission Solar Cells. *Nat. Commun.* **2012**, *3*, 1019.
46. UNSW PC1D, http://www.pv.unsw.edu.au/info-about/our-school/products-services/pc1d.
47. Lu, L.-P.; Kabra, D.; Johnson, K.; Friend, R. H. Charge-Carrier Balance and Color Purity in Polyfluorene Polymer Blends for Blue Light-Emitting Diodes. *Adv. Funct. Mater.* **2011**, *22*, 144–150.
48. Tiwana, P.; Docampo, P.; Johnston, M. B.; Herz, L. M.; Snaith, H. J. The Origin of an Efficiency Improving "Light Soaking" Effect in SnO_2 Based Solid-State Dye-Sensitized Solar Cells. *Energy Environ. Sci.* **2012**, *5*, 9566.
49. Tvrdy, K.; Frantsuzov, P. A.; Kamat, P. V. Photoinduced Electron Transfer from Semiconductor Quantum Dots to

Metal Oxide Nanoparticles. *Proc. Natl. Acad. Sci. U. S. A.* **2011**, *108*, 29–34.
50. Hyun, B.-R.; Bartnik, A. C.; Sun, L.; Hanrath, T.; Wise, F. W. Control of Electron Transfer from Lead-Salt Nanocrystals to TiO_2. *Nano Lett.* **2011**, *11*, 2126–32.
51. Goodman, A. M.; Rose, A. Double Extraction of Uniformly Generated Electron-Hole Pairs from Insulators with Non-injecting Contacts. *J. Appl. Phys.* **1971**, *42*, 2823–2830.
52. Mihailetchi, V. D.; Wildeman, J.; Blom, P. W. M. Space-Charge Limited Photocurrent. *Phys. Rev. Lett.* **2005**, *94*, 126602.
53. Ehrler, B.; Wilson, M. W. B.; Rao, A.; Friend, R. H.; Greenham, N. C. Singlet Exciton Fission-Sensitized Infrared Quantum Dot Solar Cells. *Nano Lett.* **2012**, *12*, 1053–1057.
54. Kahn, A.; Koch, N.; Gao, W. Electronic Structure and Electrical Properties of Interfaces between Metals and π-Conjugated Molecular Films. *J. Polym. Sci., Part B: Polym. Phys.* **2003**, *41*, 2529–2548.